

## Chapter 4

### Phase inversion in rotational-anisotropy SHG

#### 4.1 Introduction

We present the observation of phase inversion in RA-SHG signals. Specifically, the azimuthal angle at which a peak occurs in the RA-SHG signal switches to being one at which a valley occurs. The phase inversion can be induced by either tuning the energy of the incident photons or by surface modification, specifically the phase of H-terminated Si is inverted with respect to that of oxidized silicon at certain photon energies. The phase inversion is observed for the specific polarization configuration of *s* polarized incident light and detection of the *p* polarized SH. Such phase inversion in the presence of an applied electric field across the interface in metal-oxide-silicon structures has been reported for (*p, p*) polarization [69, 71]. RA-SHG phase inversion, without an applied electric field but rather induced by a combination of tuning of the photon energy and proper selection of the polarization configuration, has not been presented previously. We ascribe the phase inversion as function of photon energy to the presence of a resonance in the surface contribution. Because the phase is actually a relative phase between surface and bulk contributions, we conclude that this resonance must be purely a surface state that does not arise from the bulk band structure. Earlier spectroscopic studies have found resonances with this nature [59]. Furthermore, by comparing (*s, p*) data to (*q, s*) data, it is possible to distinguish the resonant behavior of  $\partial_{15}$  from that of  $\partial_{31}$ . The phase inversion due to H-termination is attributed to the change in interfacial electronic

structure as compared to the Si-SiO<sub>2</sub> interface. This is most pronounced for (*s*, *p*) polarization, although we have also observed it for (*p*, *p*) polarization, as shown in Chapter 3.

## 4.2 Experimental conditions and sample preparation

The experimental setup was the same as described in Chapter 1. RA-SHG curves were obtained by rotating the sample about the surface normal. The azimuthal angle is defined as being between plane of incidence and the [100] crystal direction. The same three samples as that in Chapter 3 were studied. They are a native oxide Si (NO-Si), a thermal oxide Si (TO-Si), and a hydrogen terminated Si (H-Si). All were prepared from the same undoped Si(001) wafer.

## 4.3 Observed phase inversions

### 4.3.1 Phase inversion due to photon energy variation

The (*s*, *p*) RA-SHG curves for the TO-Si and NO-Si samples are shown in Fig. 4.1 for a range of two-photon energies between 3.40 and 3.52 eV. The phase inversion is obvious between the curves for the lowest and highest photon energies, specifically the location of a peak in one corresponds to a valley in the other. By taking finer steps in photon energy, we can observe the phase inversion taking place. Most strikingly, we observe eightfold symmetry at one specific photon energy for each oxidized sample. Aside from the intensity, we find that the appearance of the RA-SHG signal depends sensitively on the photon energy.

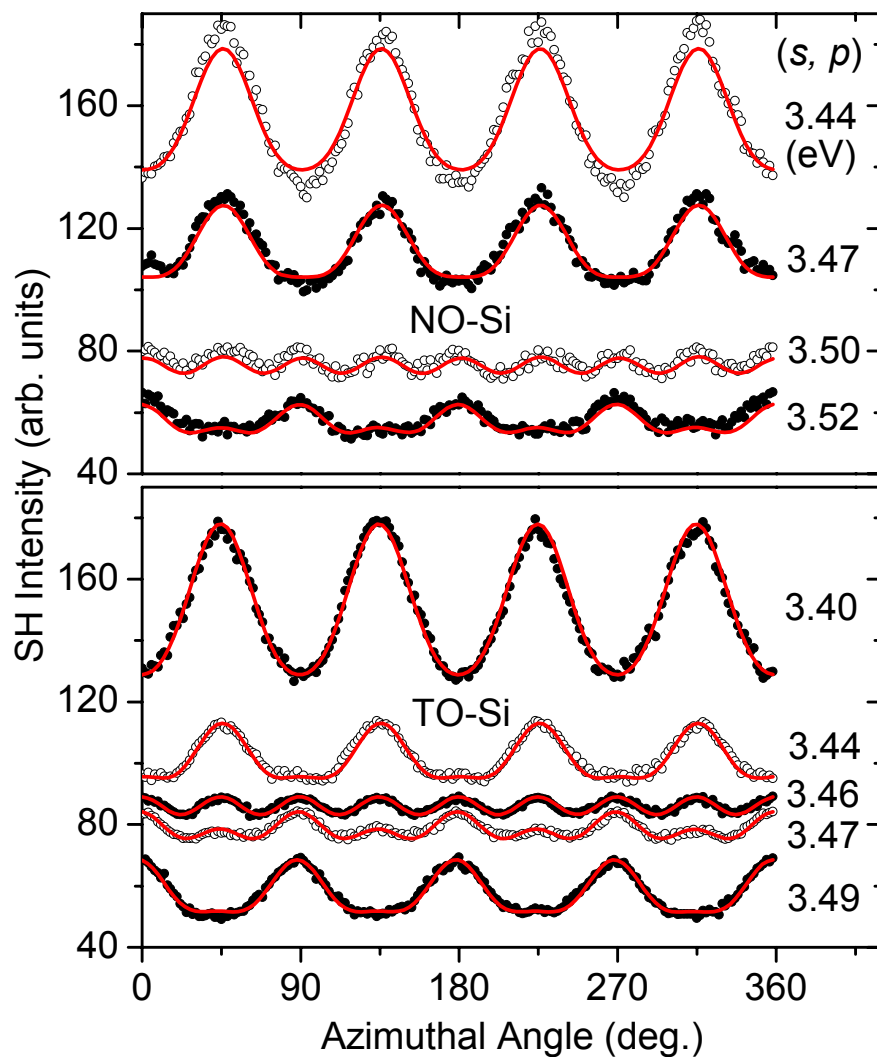


Fig. 4.1. RA-SHG signals from both NO-Si and TO-Si samples for the polarization ( $s$ ,  $p$ ) at several two-photon energies. The vertical displacement reflects the changing signal strength with two-photon energy. Note that the RA-SHG signals show eightfold symmetry at 3.50 and 3.46 eV for the NO-Si and TO-Si samples, respectively. The solid lines show the fits.

### 4.3.2 Phase inversion due to surface modification

In Fig. 4.2, we show the RA-SHG curves for all three samples at a fixed two-photon energy of 3.26 eV for both  $(s, p)$  and  $(q, s)$  polarization configurations. Here we observe that for both polarizations the phase of the H-Si sample is inverted compared to that of either oxidized sample. We have also observed that this happens for  $(p, p)$  polarization in Chapter 3 as well. To verify that doping does not play a role, we have also taken data on NO-Si samples with  $n$  and  $p$  doped substrates. They have the same phase as the oxidized samples shown in Fig. 4.2.

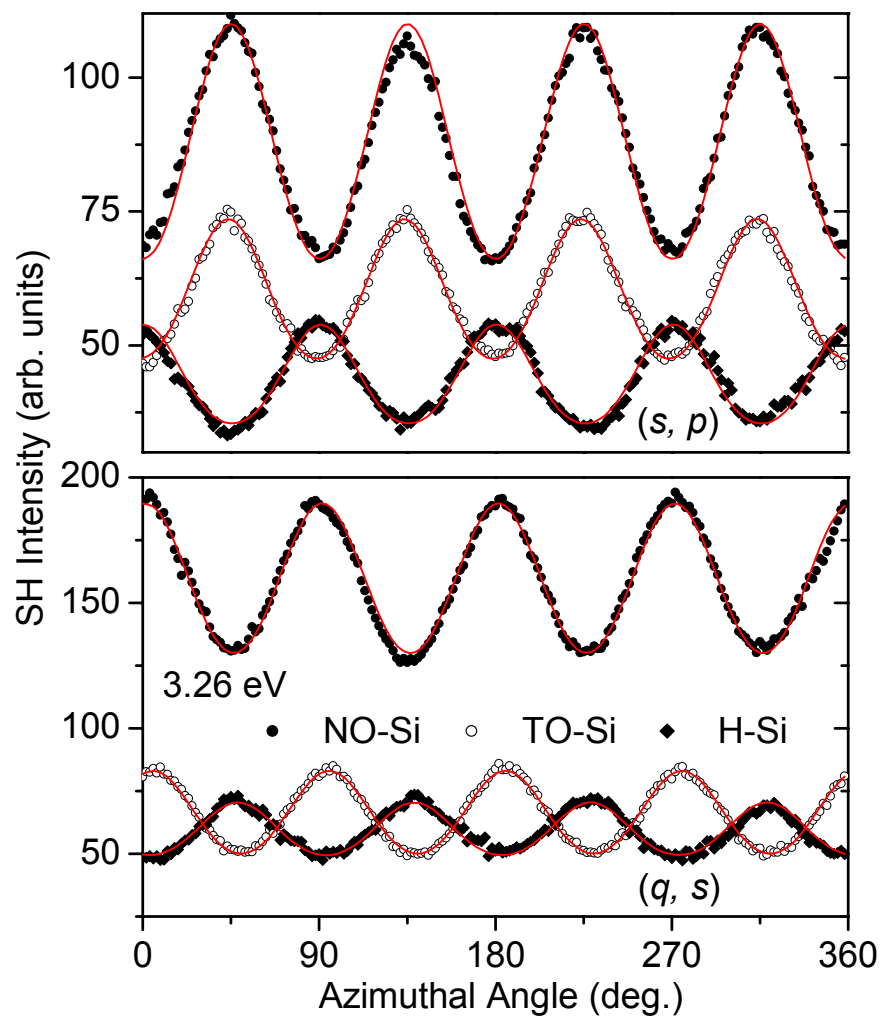


Fig. 4.2. RA-SHG intensities from modified Si(001) surfaces (NO-Si, TO-Si, and H-Si) at a two-photon energy of 3.26 eV for different polarizations:  $(s, p)$ , top panel, and  $(q, s)$ , bottom panel. Solid lines show the fits.

#### 4.4 Phase and amplitude of susceptibility tensors

To analyze the RA-SHG data, we fit the curves to theoretical predictions from Chapter 2, which shows that the SH field,  $E_{g,h}^{(2\omega)}$ , is related to the incident field,  $E_g$ , by

$$E_{s,p}^{(2\omega)} = [a_{0(s,p)} + a_{4(s,p)} \cos(4\phi)] e^{i\theta_{(s,p)}} E_s^2, \quad (4.1)$$

$$E_{q,s}^{(2\omega)} = [a_{0(q,s)} + a'_{4(q,s)} \sin(4\phi) + a_{4(q,s)} \cos(4\phi)] e^{i\theta_{(q,s)}} E_q^2, \quad (4.2)$$

where  $\phi$  is the azimuthal angle, the  $a_{n(g,h)}$ 's are the fit coefficients describing the anisotropic bulk component,  $a_{4(g,h)}$ , and the isotropic component that includes both bulk and surface contributions,  $a_{0(g,h)}$ . The intensity of the measured SH signal is proportional to the magnitude squared of the SH fields given in Eq. (4.1) or (4.2). The  $a_{4(g,h)}$  coefficients are related to each other by expressions that only involve the linear optical properties, as shown in Chapter 2. We find that the most robust procedure is to obtain  $a_{4(p,s)}$  from  $(p, s)$  data (not shown), which suppresses isotropic contributions, and then use the values of  $a_{4(s,p)}$ ,  $a_{4(q,s)}$  and  $a'_{4(q,s)}$  derived from  $a_{4(p,s)}$  in fitting the other data. The bulk anisotropic contribution was utilized as a phase reference and therefore we choose  $a_{4(g,h)}$  to be real and positive by including its phase,  $\delta_{4(g,h)}$ , in  $\theta_{(g,h)}$ . Since  $\theta_{(g,h)}$  represents an overall phase, our intensity measurements are insensitive to it. The relative phase between the bulk and surface contribution is included by allowing  $a_{0(g,h)}$  to be complex. For a given polarization configuration, we write  $a_{0(g,h)} = |a_{0(g,h)}| e^{i\delta_{0(g,h)}}$ , i.e., in terms of the magnitude and phase relative to the

anisotropic bulk component. Note that we do not determine the sign of the imaginary part of  $a_{0(g,h)}$ , which makes the sign of  $\delta_{0(g,h)}$  ambiguous. The eightfold symmetry occurs when  $a_{0(g,h)}$  is exactly  $90^\circ$  out of phase with  $a_{4(g,h)}$ , in which case there is no cross term when the intensity is calculated from Eqs. (4.1) and (4.2). The cross term has the fourfold symmetry observed in most of the traces, whereas the eightfold symmetry arises from taking the square of the  $\cos(4\phi)$  terms. Similarly, an eightfold symmetry is observed in  $(p, s)$  data where the isotropic term is suppressed entirely, also eliminating the cross term.

Based on the theory, the fit coefficients can be related to the susceptibility tensor elements. Although the actual equations, as shown in Eqs. (2.41)-(2.43) in Chapter 2, are complicated, it is sufficient to note that  $a_{0(q,s)}$  is a function of the surface element  $\partial_{15}$  and the bulk element  $\zeta$ , while  $a_{0(s,p)}$  is a function of the linear combination of surface and bulk elements  $\varepsilon(2\omega)\partial_{31} + \gamma$  and the bulk element  $\zeta$ , where  $\varepsilon(2\omega)$  is the complex dielectric constant at the frequency of the SH. The advantage of these two polarization configurations is that they isolate the two surface tensor elements  $\partial_{15}$  and  $\partial_{31}$ , whereas  $(p, p)$  yields a combination of elements. Also, since we observe that the data for the  $(s, p)$  configuration strongly depends on surface modification, we can make some separation of  $\partial_{31}$  and  $\gamma$ , because the latter is insensitive to the surface. Specifically, the phase inversion of the  $(s, p)$  signal with surface modification leads us to conclude that it is dominated by  $\partial_{31}$ ; thus we ignore  $\gamma$  in our analysis. It has been shown fundamentally that such a separation cannot be done otherwise [28].

The phase and amplitude of  $\partial_{15}$  and  $\partial_{31}$  as a function of two-photon energy obtained from the fitting are shown in Fig. 4.3 for all three samples. The phase angles of  $\zeta$ ,  $\partial_{15}$ , and  $\partial_{31}$  are designated by  $\delta_\zeta$ ,  $\delta_{15}$ , and  $\delta_{31}$ , respectively. Since there is ambiguity in the sign of the imaginary part of  $a_{0(g,h)}$ , we plot both possible values of the phases at each two-photon energy. Note that, in principle, the sign ambiguity in the fit coefficients can be lifted so that the phases of  $\partial_{31}$  and  $\partial_{15}$  can be determined uniquely, as shown in Eq. (2.50) in Chapter 2. However this requires virtually perfect polarization alignment and a better signal to noise ratio than we achieved in most of our data. By choosing to make  $a_{4(g,h)}$  real and positive, we are measuring the phases of  $\partial_{15}$  and  $\partial_{31}$  with respect to the phase of the bulk component  $\zeta$ . To obtain these tensor elements from the fit coefficients, we have calculated the linear optical coefficients from published values for the linear optical susceptibility of silicon [67]. These coefficients are complex, i.e., they result in phase shifts, thus the point of phase inversion in the signal does not correspond to  $90^\circ$  phase difference between the tensor elements. Furthermore, it means that two possible phase angles are not just different by a minus sign.

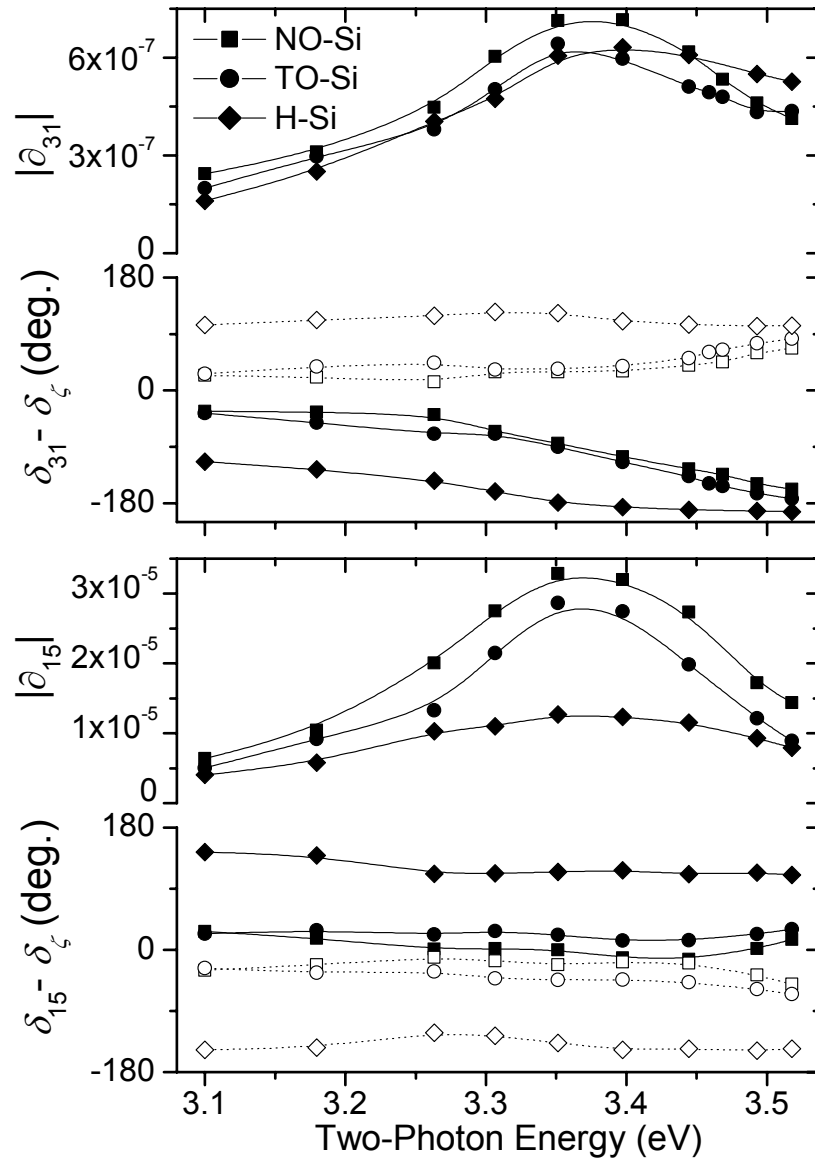


Fig. 4.3. Spectra of the amplitudes and relative phases of the tensor elements  $\partial_{31}$  (upper panel) and  $\partial_{15}$  (lower panel) for all three samples: TO-Si, NO-Si and H-Si. The amplitudes are normalized so that  $a_{4(s,s)} = 1$  at 3.26 eV. Both possible phases, arising from the ambiguity in the sign of the imaginary part of the fit coefficient, are plotted as open and filled symbols. Lines are to guide the eye.

## 4.5 Discussion

Comparing the present experimental results of SHG spectroscopy with the previous microscopic theory of SHG at Si(001) surfaces [35], we find some agreement in the resonant energy but considerable discrepancy in the magnitudes of the surface susceptibility tensor elements. Previous microscopic theories [34, 35] usually neglected the bulk SH contribution, but our results show it may significantly alter the SH spectroscopy through interference effect. From this point of view, some previous consistences between theory and experiment should be revised. For the Si-SiO<sub>2</sub> interface, we show here that SHG spectroscopy is sensitive to the sample preparation conditions and the sample azimuthal angle, and we will show in Chapter 6 that it is also sensitive to the polarization configuration. Therefore, a feasible microscopic theory to calculate the SH spectrum from a realistic Si-SiO<sub>2</sub> interface would be hard to develop and to apply to various circumstances. For hydrogen-terminated surfaces, however, the SH spectra of  $\partial_{15}$ ,  $\partial_{31}$ , and  $\partial_{33}$  have been calculated microscopically [35]; therefore, we can conveniently compare them to our experimental results. The theory and our experimental results are in agreement with that the  $(p, p)$  polarized SH contributions from all three surface tensor elements are comparable. However, our measured relative magnitude of  $\partial_{15}$  and  $\partial_{31}$  is very different from the theoretical prediction. Our results show that  $|\partial_{31}|$  is about two orders of magnitudes smaller than  $|\partial_{15}|$ , but the microscopic theory predicted that  $\partial_{15}$ ,  $\partial_{31}$ , and  $\partial_{33}$  are all comparable in magnitude. As evident in Fig. 4.2, the  $(s, p)$  and  $(q, s)$  SH intensities, which are due to  $\partial_{31}$  and  $\partial_{15}$ , respectively, are comparable

because the SH intensity is proportional to the susceptibility multiplied by its radiation factors, and not the bare susceptibility alone. Our observed peak energies of the magnitudes of  $\partial_{31}$  and  $\partial_{15}$  are very close to the theoretical prediction.

The data show the clear trend that  $\delta_{31}$  varies significantly with respect to  $\delta_{\zeta}$ , for increasing photon energy for the oxidized samples. The variation of  $\delta_{31}$  is weaker for the hydrogen terminated sample. The variation of  $\delta_{15}$  is much weaker than that of  $\delta_{31}$  for all the samples, although it appears to begin varying at the highest photon energies in the plot. Note that the magnitudes for both  $\partial_{15}$  and  $\partial_{31}$  show some degree of resonant behavior at approximately 3.38 eV for all three samples.

Change in phase with respect to driving frequency (here, the photon energy) is generally due to the presence of resonant behavior. For a simple driven oscillator, the oscillator is in phase with the driving term below resonance, lags it by  $90^\circ$  on resonance, and lags by  $180^\circ$  if the driving frequency is significantly higher than the resonance frequency. Since we are measuring the relative phase between surface and bulk terms, which also have resonances (see Chapter 3), care must be taken in interpreting the meaning of the phase; in particular, a  $90^\circ$  phase shift does not necessarily occur exactly on resonance. The observed phase inversion by photon energy has been predicted by the calculation of SH spectra using polarizable-bond model [34]. However, this phase inversion was not experimental reported before, probably due to an ambiguity in the origin of the azimuthal angle. We suggest that in the future experiments the initial direction against which one measure  $\phi$  should remain fixed throughout the whole set of frequencies.

The fact that the relative phase between  $\partial_{31}$  and  $\zeta$  is shifting with photon energy is evidence that one has a resonance that is not present in the other tensor element. Since  $\partial_{15}$  and the H-terminated sample show smaller or no phase shifts, although the bulk response should be identical, we conclude that the resonance is present in  $\partial_{31}$ . Based on the magnitude, all the tensor elements show a resonant peak around 3.38 eV. This peak has been attributed to the  $E_1$  critical point in the bulk band structure, which also appears in the surface terms due to strain imposed by the oxide layer. Since the  $E_1$  resonance is also present in the bulk response (see Chapter 3), we would expect  $\zeta$  to display a similar resonance and thus no photon energy dependent phase shifts, as occurs in the H-terminated sample. Thus  $\partial_{31}$  must have a resonance that is not present in the bulk.

Spectroscopic measurements that only measured the amplitude of the SHG signal, and not its phase, showed the existence of resonances at higher photon energies [59]. Based only on the energetics of these resonances, it was concluded that they must be due to transitions that were unique to the interface as there are no equivalent bulk transitions. Since  $(p, p)$  polarization was used, the resonant behavior of the SH intensity was a combined effect of the interface (including  $\partial_{31}$ ,  $\partial_{33}$ , and  $\partial_{15}$ ) and bulk contributions. Our separation of individual tensor elements reveals the effect of excitation orientation. As shown in Fig. 4.3, the resonant energy of  $\partial_{31}$  discriminates different strains at the interface because the resonant energies of  $\partial_{31}$  increases from TO-Si to NO-Si then to H-Si. The amplitude of  $\partial_{15}$  is most sensitive to the difference between oxidized and hydrogen terminated surfaces. This indicates

that in-plane excitation probes the interfacial strain while out-of-plane excitation probes the interfacial bond. The presence of interface only transitions explains the shift in the relative phase between the surface and bulk contributions that we observe. Furthermore, our phase measurements prove that there are transitions that are only due to the interface and do not occur in the bulk, otherwise there would not be a phase shift.

For low photon energy, i.e., below the  $E_1$  resonance, there is a consistent phase shift between the oxidized samples and the H-terminated sample. We attribute this to the difference in the electronic structure of the H-Si interface compared to that of the SiO<sub>2</sub>-Si interface. Specifically, O is substantially more electronegative than H. Although the actual interface bonds are not resonant at these photon energies, it has been shown theoretically that simply changing the electronegativity of ad-atoms can dramatically change the spectrum of SHG [72]. Although this study did not address the phase of the SHG, it would be expected that it would also be affected. This is presumably due to modification of the band structure of the first few monolayers of the crystal, which is consistent with the fact that phase inversion can be induced by a dc electric field across the SiO<sub>2</sub>-Si interface [69, 71].

#### **4.6 Summary**

We have shown that the RA-SHG signals provide information about the relative phase of the surface or interface tensor elements compared to the bulk elements. The phase of the azimuthal dependence of second harmonic generation from Si(001) interfaces is observed to undergo an inversion for appropriate

polarization configurations. The azimuthal dependence is due to interference between second harmonic generation from bulk anisotropic tensor elements and isotropic elements, which include both bulk and surface terms. The inversion can be induced by either varying the photon energy or by surface modification. In the former case, the inversion is ascribed to the presence of a resonance in the surface contribution and it enhances the ability to identify resonance positions. The photon energy dependence of the phase reveals resonances that are only present in the Si-SiO<sub>2</sub> interface and have no equivalent in the band structure of the bulk. The careful analysis presented here shows that significantly more information can be extracted from RA-SHG scans, particularly with regard to separating the bulk and surface contributions, than has been done heretofore.